THE JOURNAL OF PHYSICAL CHEMISTRY C

Article

pubs.acs.org/JPCC

Ab Initio Study of Stability of $Na_2Fe_2(SO_4)_3$, a High Potential Na-Ion Battery Cathode Material

Maxim Shishkin*,† and Hirofumi Sato†,‡

†Elements Strategy Initiative for Catalysts and Batteries (ESICB), Kyoto University, Nishikyo-ku, Kyoto 615-8520, Japan

‡Department of Molecular Engineering, Kyoto University, Nishikyo-ku, Kyoto 615-8510, Japan

ABSTRACT: The free energies of thermal decomposition and hydration of $Na_2Fe_2(SO_4)_3$, used as a high operating potential Na-ion battery cathode material (3.8 V), are calculated with the help of the DFT+U method, augmented by magnetic exchange term. In addition, the energetics of hydration of low potential $Na_2Fe(SO_4)\cdot 2H_2O$ cathode (3.25 V) in humidified atmosphere is also analyzed. We find that DFT+U/magnetic exchange method can provide a reasonable agreement between calculated ground state properties of the studied materials (i.e., energetics and magnetic moments) and experiment. Using the evaluated total energies of solid materials and the free energies of the molecular species, we determined that $Na_2Fe_2(SO_4)_3$ is indeed thermally unstable at temperatures $T \sim 450$ °C in agreement with experimental observations. Moreover, our calculations predict that $Na_2Fe_2(SO_4)_3$ can be hydrated in room temperature environment ($T = 20$ °C) also in a reasonable agreement with experiment. Overall, our work shows that the DFT+U method, augmented by magnetic exchange, can be used for analysis of thermal decomposition and hydration of complex compounds such as Na intercalated iron sulfates.

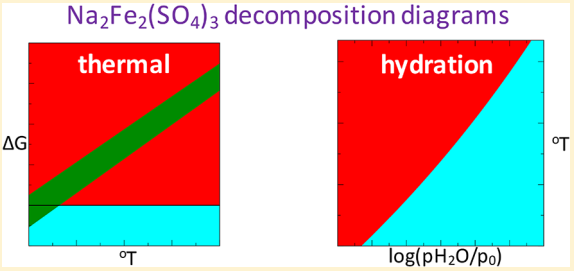

1. INTRODUCTION

Metal sulfates (e.g., Na_2SO_4 or $FeSO_4$) find a wide range of applications in chemical industry including corrosion resistance, thermal storage, paper pulping, ink production, and many more. Recently sulfates of transition metals have attracted substantial interest as cathode materials in Li- and Na-ion batteries mostly due to their very high operating potential as compared to other compounds such as oxides, phosphates, silicates, and borates.[1−3] Higher operating (redox) potentials of sulfates are usually attributed to the inductive effect, i.e., a higher potential of a material redox couple is caused by a more electronegative polyatomic anion of a sulfate (i.e., SO_4^{2-}) as compared to less electronegative counterparts such as PO_4^{3-}, BO_3^{3-}, and SiO_4^{4-}.[4]

The most prominent example of a sulfate cathode material is Na intercalated iron sulfate, $Na_2Fe_2(SO_4)_3$, which possesses a rather high average operating potential (3.8 V), stability of redox cycling, and low barriers for Na ion migration[5] (the actual stoichiometry of this material is $Na_{2.304}Fe_{1.848}(SO_4)_3$, which differs from the commonly used formula due to the presence of partially occupied Na and Fe sites as discussed in ref 5). Inspired by these promising properties of iron sulfates, several groups attempted to develop even higher operating potential cathodes via substitution of Fe with other cations (e.g., Mn or Co in refs 6 and 7 respectively). However, although respective materials were successfully synthesized, much poorer electrochemical properties prevent these structures from being competitive alternatives to $Na_2Fe_2(SO_4)_3$ prototype, at least to date.

In addition to electrochemical characteristics, another important property of the cathode materials is their stability in various ranges of temperature and resistance to moisture present in the air. For instance, $Na_2Fe_2(SO_4)_3$ is reported to be unstable at temperatures above 450 °C resulting in decomposition into Na_2SO_4, Fe_2O_3, Fe_3O_4, and SO_2.[5] Moreover, interactions between the water molecules, present in the air, and $Na_2Fe_2(SO_4)_3$ results in formation of a hydrated product $Na_2Fe(SO_4)_2\cdot 4H_2O$.[5] Understanding of the mechanisms and driving factors responsible for these undesirable reactions is clearly a prerequisite for the design of stable cathode materials. From the modeling perspective, a computational framework, which allows accurate evaluation of both electrochemical and stability properties of cathode materials, should be formulated and applied.

The key quantities that need to be evaluated for analysis of stability properties of materials are enthalpies of formation and oxidation. For the case of transition metal compounds, calculations of these properties is a challenging task, owing to inability of the widely used local DFT functionals (LDA and GGA) to accurately describe the electronic structure of strongly correlated materials.[8] As a remedy, Hubbard corrected DFT+U method, which provides more realistic charge distribution of the strongly localized d- and f-electron states (as compared to LDA or GGA), is often used.[9] One of the key challenges associated with applying the DFT+U method is determination

Received: March 16, 2017
Revised: August 28, 2017
Published: August 29, 2017

DOI: 10.1021/acs.jpcc.7b02479
J. Phys. Chem. C 2017, 121, 20067−20074

of a numerical U parameter, which has to be adopted for calculation of energetics and electronic structure of materials. The values of U are usually determined with the help of a fitting procedure, where U parameter is adjusted to reproduce experimentally measured characteristics such as formation enthalpies or band gaps.[10−13] Alternatively, U parameters can be evaluated computationally, avoiding any fitting to the results of experimental measurements.[14−20] In our previous work, we performed an evaluation of redox potentials of several oxide and phosphate materials using linear response approach with self-consistent calculation of U parameters.[21] We have shown that for insulating materials this method can provide values of redox potentials in a very reasonable agreement with experiment.[21]

However, in our more recent work,[22] where we attempted application of DFT+U/linear response approach to three iron sulfate materials, we found that calculated redox potentials are significantly overestimated (by more than 0.5 V as compared to the measured values). We attributed this discrepancy to inadequate evaluation of magnetic moments of intercalated structures, as our calculations revealed that magnetic moments for $Li_2Fe(SO_4)_2$, determined by DFT+U method, are by 0.44 μ_B higher than experimental, whereas for deintercalated phase ($LiFe(SO_4)_2$) the difference is only 0.1 μ_B.[22] As a possible solution we recalculated total energies and magnetic structures using the DFT+U method, augmented by magnetic exchange term which introduces additional interactions between the electrons with opposite spins, localized on transition metal (TM) ions (i.e., Fe).[22] Our calculations revealed that both redox potentials and magnetic properties of intercalated structure can be brought to a much better agreement with experiment as compared to DFT+U calculations, where reasonable match with experiment for only one of these quantities (either redox potential or magnetic moment) can be achieved by varying the value of U.[22]

The aim of this work is application of the DFT+U method, augmented by magnetic exchange to the analysis of stability of Fe-based sulfate cathode materials. Particularly, we studied decomposition of the high potential $Na_2Fe_2(SO_4)_3$ cathode at elevated temperatures (300 °C < T < 500 °C) and its hydration when exposed to gas phase water molecules present in the air. We also performed a study of the reaction of hydration of low potential $NaFe_2(SO_4)_2{\cdot}2H_2O$ cathode. Before presenting the results of our findings, we wish to provide a brief overview of the subsequent sections. In section 2 we give a description of DFT+U formalism as well as magnetic exchange contribution. In subsection 3.1 we discuss the results of a study of Fe_2O_3 and Fe_3O_4 as these two materials are the products of thermal decomposition of $Na_2Fe_2(SO_4)_3$. Particularly, we evaluated magnetic moments of Fe ions and enthalpy of Fe_3O_4 oxidation with formation of Fe_2O_3 using DFT+U and DFT+U method augmented by magnetic exchange. In subsection 3.2 we present an analysis of the free energy of $Na_2Fe_2(SO_4)_3$ decomposition as a function of temperature, thus allowing determination of a temperature range where this cathode material is thermodynamically unstable. In subsection 3.3 we present the results of calculations of the free energy of $Na_2Fe_2(SO_4)_3$ hydration as a function of temperature and partial pressure of H_2O. We also performed a similar analysis for the $NaFe_2(SO_4)_2{\cdot}2H_2O$ cathode material. Conclusions of this work are summarized in section 4.

2. METHODOLOGY DESCRIPTION

Calculations of energetics as well as electronic structure and magnetic moments of studied materials have been performed using the VASP ab initio package.[23] PBE functional has been used for treatment of exchange correlation effects,[24] and projector augmented wave (PAW) formalism[25,26] has been employed for description of electron−nuclear interactions. We used a high cutoff energy of 800 eV for the plane wave expansion of electronic states and Monkhorst−Pack method[27] for the Brillouin zone sampling. The specific k-point mesh for each studied material has been chosen to provide well converged values of studied total energy differences (below 0.01 eV per formula unit).

In view of the well recognized limitations of the local exchange correlation functionals in treatment of strongly localized d- and f-electronic states, in this work we employed Hubbard corrected DFT+U method which allows more accurate description of the d-states of Fe cations.[28] Within DFT+U approach, the energy of an atomic system is calculated via correction of the energy E^{DFT}, determined by the local DFT method:

$$E^{DFT+U}[n(\mathbf{r})] = E^{DFT}[n(\mathbf{r})] + E^{Hub}[\mathbf{n}^{I\sigma}] - E^{DC}[N^{I\sigma}] \quad (1)$$

In the above expression the Hubbard correction term (E^{Hub}) is added to provide more accurate description of the interactions between the localized d-electrons whereas E^{DC} is a double counting correction that needs to be subtracted to remove interactions between d-electrons, calculated using a local (e.g., PBE) functional. Within Dudarev's approximation,[29] employed herein the combined Hubbard and double counting correction term has the following expression

$$E^{U_{eff}}[\mathbf{n}^{I\sigma}] = \sum_{I,\sigma} \frac{U^I_{eff}}{2} Tr[\mathbf{n}^{I\sigma}(1 - \mathbf{n}^{I\sigma})] \quad (2)$$

where U^I_{eff} is an effective Hubbard parameter and $\mathbf{n}^{I\sigma}$ is an occupation matrix, elements of which can be evaluated as

$$n^{I\sigma}_{mm'} = \sum_{\mathbf{k},v} f^{\sigma}_{\mathbf{k},v} \langle \psi^{\sigma}_{\mathbf{k},v} | P^I_{mm'} | \psi^{\sigma}_{\mathbf{k},v} \rangle \quad (3)$$

In the above expression, $|\psi^{\sigma}_{\mathbf{k},v}\rangle$ are the single electron bands ($\mathbf{k}$ and v are the k-point and the band number indices whereas σ is a spin index), $f^{\sigma}_{\mathbf{k},v}$ are the occupation numbers, and $P^I_{mm'}$ are the operators of single electron band projectors on d-states:

$$P^I_{mm'} = |\phi^I_m\rangle\langle\phi^I_{m'}| \quad (4)$$

In eqs 3 and 4 I is an index which denotes an ion with Hubbard corrected localized states (i.e., Fe cations in our case). The Hubbard contribution operator that needs to be added to the DFT Hamiltonian can be obtained via a simple derivative of the functional (eq 2) over density:

$$V^{U_{eff}}|\psi^{\sigma}_{\mathbf{k},v}\rangle = \sum_{I,m,m'} U^I_{eff}\left(\frac{1}{2}\delta_{mm'} - n^{I\sigma}_{mm'}\right)|\phi^I_{m'}\rangle\langle\phi^I_m|\psi^{\sigma}_{\mathbf{k},v}\rangle \quad (5)$$

In this work, the values of U_{eff} parameters have been evaluated using linear response method, whose description can be found elsewhere.[21,30]

The Hubbard correction in eqs 2 and 5 accounts for only interactions between the electrons of the same spin. In some cases, particularly when substantial numbers of electrons, localized on the same atom (I), are present in both majority

DOI: 10.1021/acs.jpcc.7b02479
J. Phys. Chem. C 2017, 121, 20067−20074

and minority spin channels, it might be reasonable to introduce an additional term,[22,31] which accounts for the interactions between the states of the opposite spin:

$$E[\mathbf{n}^{\sigma}] = \sum_{\sigma} \frac{U-J}{2} Tr[\mathbf{n}^{\sigma}(1-\mathbf{n}^{\sigma})] - \sum_{\sigma} \frac{J}{2} Tr[\mathbf{n}^{\sigma}\mathbf{n}^{\bar{\sigma}}] + E^{\mathrm{DC}} \quad (6)$$

The additional double counting correction is introduced in eq 6 due to the presence of the new term, thus resulting in the following expression for the Hubbard correction functional

$$E[\mathbf{n}^{\sigma}, \mathbf{m}] = \sum_{\sigma} \frac{U}{2} Tr[\mathbf{n}^{\sigma}(1-\mathbf{n}^{\sigma})] + \frac{J}{2} Tr[\mathbf{m}(\mathbf{m}-1)] \quad (7)$$

where $\mathbf{m}$ is a magnetization matrix, defined as $\mathbf{m} = \mathbf{n}^{\sigma} - \mathbf{n}^{\bar{\sigma}}$.

The need for extension of the common Hubbard correction term (eqs 2 and 5) has been realized previously, and several works employing this extended method have been published to date (see the papers, citing ref 31). In our recent work we have shown that application of DFT+U method, augmented by the magnetic exchange contribution (eqs 6 and 7), is necessary for accurate description of the redox properties and magnetic structure of iron sulfate cathode materials of Na-ion batteries.[22] Herein, DFT+U method, augmented by the magnetic exchange, is further used for the study of stability properties of iron sulfates and oxides as well as for calculation of magnetic properties of iron oxides. Similar to this previous work,[22] we fixed U_{eff} to the values determined via linear response calculations and varied the values of J parameters for the better agreement of theoretically calculated magnetic and redox properties of studied materials with experimental data. As a special note, we also wish to mention that the values of J parameters presented in ref 22 have to be devided by 2.[32] These corrections do not change the results and conclusions provided in ref 22.

3. RESULTS AND DISCUSSION

3.1. Analysis of the Properties of Fe_2O_3 and Fe_3O_4.

Fe_2O_3 and Fe_3O_4 belong to the group of important functional materials which have been studied extensively. As both of these oxides are the products of thermal decomposition of $Na_2Fe_2(SO_4)_3$, in this work we are interested in accurate evaluation of their ground state properties such as energetics and magnetic moments of iron cations. The structures of studied materials are shown in Figure 1: Fe_2O_3 adopts a hematite and Fe_3O_4 a cubic magnetite configuration. In our calculations we have chosen magnetic ordering that corresponds to the minimum energy (ground state) for each material. More specifically, antiferromagnetic G-type ordering has been imposed on Fe_2O_3[33] whereas, for the case of Fe_3O_4, positive magnetic moments were imposed on Fe ions with tetrahedral cage of oxygens (A sites) and negative moments on Fe ions with octahedral cage of oxygens (B sites).[34]

As an indicator of the accuracy of calculated energies of these oxides, we select an enthalpy of Fe_3O_4 oxidation with formation of Fe_2O_3:

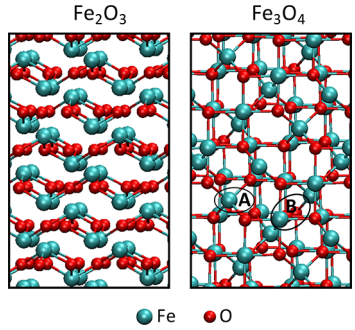

Figure 1. Optimized structures of Fe_2O_3 and Fe_3O_4 oxides. The A and B iron sites of Fe_3O_4 have positive and negative magnetic moments respectively (see the text for details).

$$\frac{2}{3}Fe_3O_4 + \frac{1}{6}O_2 \rightarrow Fe_2O_3 \quad (8)$$

Using experimental values for the enthalpies of formation of both oxides[35]

$$H(Fe_2O_3) - 2H(Fe) - \frac{3}{2}H(O_2) = -822\ \mathrm{kJ/mol}$$
$$H(Fe_3O_4) - 3H(Fe) - 2H(O_2) = -1121\ \mathrm{kJ/mol} \quad (9)$$

one can easily find that the enthalpy of Fe_3O_4 oxidation (eq 8) is −0.77 eV. In this section we applied several methods for evaluation of an enthalpy of the reaction in eq 8 as discussed below.

Prior to discussion of our results, several remarks should be added with regard to calculation of the energy of oxygen molecule (O_2). The energy of this molecule in the triplet ground state is known to be too low when DFT calculations are adopted; therefore, corrections are usually employed for more adequate value of $H(O_2)$. Such corrected value of $H(O_2)$ has been estimated in the past via fitting the energy of formation of various oxides to experiment.[36] One of us has previously introduced such type of correction, reporting the value of $H(O_2)$ equal to −8.35 eV.[37] In this work, however, we are using a slightly lower value of −8.55 eV for the two following reasons: (a) it can be used to accurately reproduce the energy of atomization of oxygen molecule as compared to experiment (our calculations predict the value of 2.59 eV in excellent agreement with experiment, which is 2.58 eV[38]); (b) it is in a very good agreement with the value suggested in previous works (−8.5 eV),[10,39] where fitting approach to the experimental enthalpies of oxidation reactions has been applied.

Now we proceed to the analysis of calculated properties of Fe_2O_3 and Fe_3O_4 (Table 1). Calculations have been performed using the following methods: (a) DFT+U/linear response (LR)[21] (the employed U values are 3.54 and 4.32 eV for Fe_2O_3 and Fe_3O_4, respectively); (b) DFT+U with magnetic moments of Fe fitted to experiment;[33,40] (c) DFT+U with the recommended value of U (U = 4 eV), previously derived using a fitting procedure;[10,11] (d) DFT+U with magnetic exchange[22] (J = −4.0 and 2.0 eV for Fe_2O_3 and Fe_3O_4 respectively, whereas U values are identical to those found by the LR method). In addition to calculated enthalpy of Fe_3O_4 oxidation, we also present the magnetic moments of Fe in both oxides[33,40] and the band gap of Fe_2O_3[33] (Fe_3O_4 is a semimetal) for comparison with reported experimental values.

Our results show that within DFT+U/LR approximation, the energy of Fe_3O_4 oxidation is quite underestimated. Moreover,

DOI: 10.1021/acs.jpcc.7b02479
J. Phys. Chem. C 2017, 121, 20067−20074

Table 1. Values of Enthalpy of Fe_3O_4 Oxidation (ΔH), Magnetic Moments of Fe Cations in Both Studied Iron Oxides and the Band Gap of Fe_2O_3 Calculated Using Various Computational Methods[a]

method	properties			
	ΔH (eV)	$\mu_B(Fe_2O_3)$	$\mu_B(Fe_3O_4)$	gap (eV)
DFT+U/LR	−1.67	4.08	4.04	1.5
DFT+U/μ_{fit}	2.78	4.47	3.81	3.0
DFT+U (U = 4 eV)	−1.10	4.13	4.02	1.7
DFT+U/mag.exch.	−0.78	4.53	3.7	3.2
experiment	−0.77	4.64[33]	3.68[40]	2.2[33]

[a]We used U = 3.54 eV, J = −4 eV for Fe_2O_3 and U = 4.32 eV, J = 2 eV for Fe_3O_4. Experimental values are provided for comparison.

both magnetic moments of Fe deviate from experiment substantially whereas the band gap of Fe_2O_3 is underestimated. Thus, DFT+U/LR calculations predict quite inaccurate energetics and magnetic structure for these oxides. We also find that an attempt of fitting the magnetic moments of Fe to experimental values results in a very unrealistic prediction of the enthalpy of Fe_3O_4 oxidation. Moreover, the band gap of Fe_2O_3 in this case is found to be much wider than experimentally measured. On the other hand, when using the recommended value of U = 4 eV,[10] we find that the enthalpy of Fe_3O_4 oxidation is in closer agreement with experiment as compared to DFT+U/LR result, although it is still underestimated. Moreover, the magnetic moments deviate from experimental measurements by a significant margin.

Table 1 clearly demonstrates that a good agreement with experiment for calculated enthalpy of oxidation and magnetic moments can be achieved only in case when DFT+U with magnetic exchange approach is applied (in this work the U_{eff} parameters have been calculated using linear response approach,[21] whereas J parameters have been adjusted subsequently to bring the calculated magnetic moments to a better agreement with experimental values). Indeed, absolute values of magnetic moments of Fe cations are in much closer agreement with experimental measurements than those of DFT+U/LR calculations. Such adequate shifts in the magnitudes of μ_{Fe} are caused by introduced J parameters in the DFT+U/mag. exchange method. Moreover, addition of magnetic exchange also results in a higher value of the enthalpy of Fe_3O_4 oxidation, as compared to DFT+U/LR approach, bringing it to a closer agreement with experiment.

The impact of inclusion of magnetic exchange term into DFT+U functional on the electronic structure of studied materials can be analyzed using Figure 2. In the case of Fe_2O_3, the peak of the majority d-states of Fe cations is shifted downward in energy, thus accounting for a larger magnitude of magnetic moment of Fe cations as compared to DFT+U calculations (see also Table 1). On the other hand, for the case of Fe_3O_4, the majority d-states of Fe cations are clearly shifted upward in energy, resulting in lower values of magnetic moments on both A and B sites.

Figure 2 also shows that the band gap of Fe_2O_3 is widened upon inclusion of magnetic exchange interaction. This effect is very similar to the usual trend, observed in application of DFT+U scheme, where greater degree of localization of d-states is introduced alongside with a wider theoretical band gap (as compared to DFT). In general we find that the width of the band gap changes monotonically with J parameter, similar to the case of variation of U in the standard DFT+U calculations.

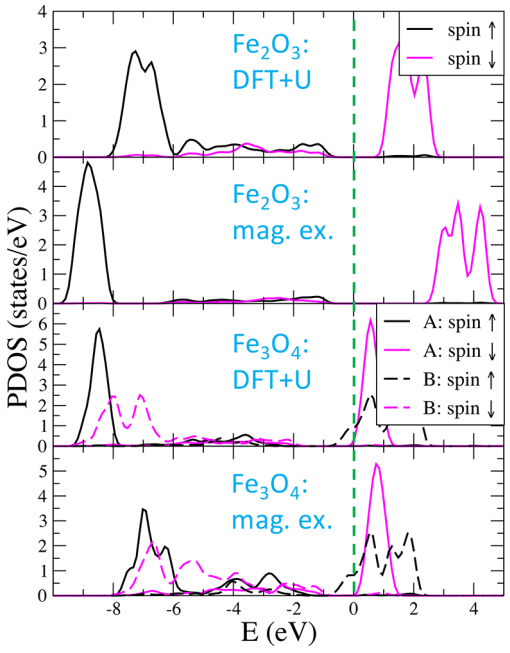

Figure 2. PDOS of d-states of selected Fe cations of Fe_2O_3 (two upper panels) and Fe_3O_4 (two lower panels) determined by DFT+U and DFT+U with magnetic exchange methods. The Fermi level is indicated by the broken vertical line. The majority spin up states are shown with black color, whereas minority spin down states with magenta color. The PDOS for A and B sites of Fe_3O_4 are given by solid and broken lines, respectively.

Similarly magnetic moment is also a monotonic function of J parameter. Overall, our calculations show that employed schemes can provide good approximations for description of the ground state properties (e.g., enthalpies of formation and magentic moments), whereas an ability of prediction of the properties of unoccupied states, such as band gap, is clearly lower (for Fe_2O_3, the respective value is greater than the actual experimental gap (Table 1)). For this reason, in the next subsection, where we studied thermal decomposition of $Na_2Fe_2(SO_4)_3$, we used the total energies of Fe_2O_3 and Fe_3O_4 products obtained with the help of DFT+U/magnetic exchange approach.

3.2. Thermal Decomposition of $Na_2Fe_2(SO_4)_3$. As we have already mentioned in the Introduction, the $Na_2Fe_2(SO_4)_3$ (the optimized structure is shown in Figure 3) is found to decompose at temperatures above 450 °C into Na_2SO_4, Fe_2O_3,

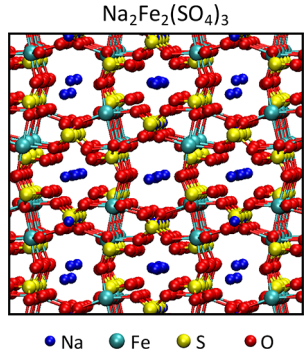

Figure 3. Optimized structure of $Na_2Fe_2(SO_4)_3$.

DOI: 10.1021/acs.jpcc.7b02479
J. Phys. Chem. C 2017, 121, 20067−20074

and Fe_3O_4 solids and O_2 and SO_2 gas phase molecules.[5] The equation for this reaction can be written as

$$Na_{18}Fe_{15}(SO_4)_{24} \xrightarrow{T>450^\circ C} 9Na_2SO_4 + 15gSO_2 + 15\left\{\frac{1-3y}{2}Fe_2O_3 + yFe_3O_4 + \frac{y+1}{4}gO_2\right\} \quad (10)$$

In eq 10 the stoichiometry of the computational cell ($Na_{2.25}Fe_{1.875}(SO_4)_3$) is reasonably close to the experimental ($Na_{2.304}Fe_{1.848}(SO_4)_3$) (we used the lowest total energies of the analyzed configurations for all structures with partial site occupancies; the types of the employed cells of the Fe sulfates are identical to those described in ref 22.). The coefficient y is introduced into eq 10 to reflect possible relative amounts of Fe_2O_3 and Fe_3O_4 oxides. Clearly, y can only lie in the range $0 < y < 1/3$, where $y = 0$ corresponds to formation of Fe_2O_3 exclusively (i.e., no Fe_3O_4 is formed), whereas $y = 1/3$ corresponds to exclusive formation of Fe_3O_4 (with no formation of Fe_2O_3).

For calculations of total energies of $Na_2Fe_2(SO_4)_3$, Fe_2O_3, and Fe_3O_4, we used DFT+U/magnetic exchange approach as discussed in the Introduction and the previous section. Moreover, a corrected value of the total energy of O_2 is used. As for Na_2SO_4 and SO_2, we performed standard evaluation of their total energies using PBE calculations.

Our analysis of $Na_2Fe_2(SO_4)_3$ decomposition (eq 10) aims at determination of the conditions where the combined free energy of the reactants becomes higher than the combined free energy of the products. Within this work we adopted an approximation that the free energies of solids are equal to their enthalpies.[41,42] For molecules the free energies are evaluated as

$$G(T, p) = H_{DFT} + RT\ln\left(\frac{p}{p_0}\right) - TS(T, p_0) \quad (11)$$

where p is a partial pressure of each studied species and T is an ambient temperature; S is an entropy of the gas phase species; R is a Boltzmann constant; and p_0 is a reference atmospheric pressure. We assigned equilibrium partial pressures of O_2 and SO_2 to normal atmospheric: $0.2p_0$ for O_2 and 1 ppb for SO_2. Although entropy is a function of T in eq 11, in the free energy calculations we used constant values of entropy for both SO_2 and O_2 molecules at $T = 700$ K. This approximation is reasonable, given a very small change of S in the range $600\ K < T < 800\ K$, which is considered well below the error bars of the calculated energies of the other involved species.

The difference between the free energy of $Na_2Fe_2(SO_4)_3$ and the products of its decomposition (ΔG) is shown in Figure 4 (ΔG is essentially the free energy of a $Na_2Fe_2(SO_4)_3$ formation). The green segment corresponds to the values of ΔG as a function of temperature (T) and parameter y in eq 10 (partial pressures of O_2 and SO_2 are kept fixed). To facilitate our analysis, the red region in Figure 4 corresponds to the conditions where decomposition is thermodynamically favorable ($\Delta G > 0$), whereas the blue region corresponds to the conditions where $Na_2Fe_2(SO_4)_3$ remains stable. As expected, we find that decomposition of $Na_2Fe_2(SO_4)_3$ becomes more favorable at higher temperatures (Figure 4). We also find that

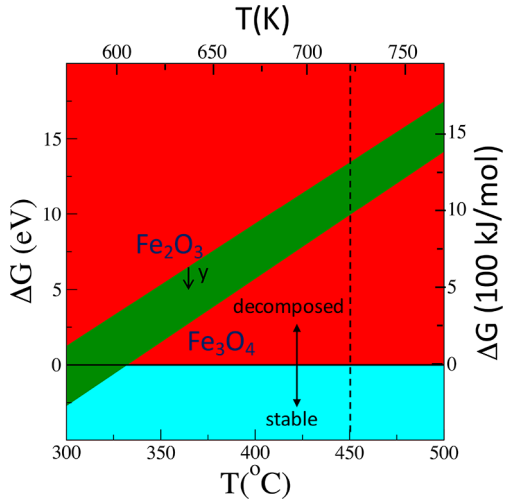

Figure 4. Free energy of thermal decomposition of $Na_2Fe_2(SO_4)_3$ as a function of ambient temperature. The green segment covers the possible values of ΔG. Upper and lower boundaries of the green segment correspond to the exclusive formation of Fe_2O_3 and Fe_3O_4 products, respectively.

formation of Fe_3O_4 is thermodynamically more favorable than Fe_2O_3. Overall the predicted temperature of $Na_2Fe_2(SO_4)_3$ decomposition ($T \sim 320$ °C) is significantly lower than the experimental (450 °C).[5] We wish to comment on possible reasons of this underestimated value of the temperature of decomposition.

First it is possible that calculations of total energies of Na_2SO_4 and SO_2 using PBE approximation may not be accurate enough. Indeed, atomization of SO_2 is known to be poorly described by the local DFT methods.[43] A second possible reason might be high kinetic barriers within the reaction in eq 10, thus requiring even higher temperature of thermal decomposition.

Overall, we find that using the energies of all involved species, calculated by DFT or DFT+U/magnetic exchange methods, we can predict that $Na_2Fe_2(SO_4)_3$ is unstable at high temperatures. However, the calculated temperature of decomposition is by about 130 K lower than experimental. This shows that employed approach can be used only for determination of the qualitative trends, whereas specific temperatures of the process may not be calculated precisely.

3.3. Hydration of $Na_2Fe_2(SO_4)_3$ and $Na_2Fe(SO_4)_2\cdot 2(H_2O)$. Hydration of $Na_2Fe_2(SO_4)_3$ with formation of $Na_2Fe(SO_4)_2\cdot 4(H_2O)$ (whose optimized structure is shown in Figure 5) has been observed[5] upon exposure of this cathode material to the air according to the following reaction mechanism:

$$Na_{18}Fe_{15}(SO_4)_{24} + 36gH_2O \rightarrow 9Na_2Fe(SO_4)_2\cdot 4(H_2O) + 6FeSO_4 \quad (12)$$

As in the previous section, we wish to comment on calculations of total energies of the products of the reaction in eq 12. The hydrated sulfate is known to be a cathode material with reported average redox potential of 3.3 V.[44] Similar to the other sulfate cathodes studied by us, we find that DFT/LR predicts a rather overestimated redox potential of 3.8 V. On the other hand, when the magnetic exchange contribution is added ($J = 3$ eV), the calculated redox potential of $Na_2Fe(SO_4)_2\cdot 4(H_2O)$ is 3.4 V, which is in a reasonable

DOI: 10.1021/acs.jpcc.7b02479
J. Phys. Chem. C 2017, 121, 20067−20074

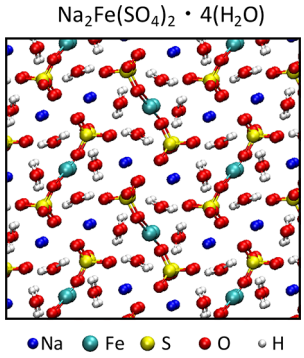

Figure 5. Optimized structure of $Na_2Fe(SO_4)_2{\cdot}4(H_2O)$.

agreement with experiment. We also note that the absolute values of magnetic moments of Fe of hydrated structure are lower as compared to these determined by DFT+U/LR calculations in full agreement with the studies on other sulfates.[22]

DFT+U calculations with magnetic exchange contribution (J = 3 eV) have been also applied to $FeSO_4$ for evaluation of its total energy in view of the same oxidation state of Fe in this material as in other sulfates (eq 12). This approximation has been adopted as we were not able to find redox potentials or spin magnetic moments of Fe for this material. Thus, for all sulfates in eq 12, DFT+U with magnetic exchange contribution (J = 3 eV) has been used, whereas PBE calculations have been employed for calculation of the total energy of a water molecule.

For evaluation of the free energy of the reaction in eq 12 (ΔG, which is equal to the free energy of the products minus the free energy of the reactants), we used the same approach as outlined in the previous section: the free energies of solids are approximated to be equal to their respective enthalpies, and the free energy of a gas phase H_2O is determined using eq 11. In calculation of the free energy of H_2O, we used the value of entropy at T = 20 °C and $p = p_0$.

Figure 6 presents the results of our calculations: the red and blue areas correspond to the values of temperature (T) and partial pressure of water (p) where reaction ΔG is positive and negative, respectively. Positive ΔG indicates that hydration is unfavorable and thus $Na_2Fe_2(SO_4)_3$ is stable, whereas negative ΔG corresponds to the conditions (T and p of water) under which hydration of $Na_2Fe_2(SO_4)_3$ is favorable. In Figure 6 we also show the vapor pressure of water (black solid line), which indicates the maximum partial pressures of gas phase water prior to condensation at each specific temperature. Therefore, only the region to the left of the solid line in Figure 6 should be analyzed, as in this study we are interested in analysis of interactions of the gas phase water with $Na_2Fe_2(SO_4)_3$.

Figure 6 shows that $Na_2Fe_2(SO_4)_3$ cathode material is more stable at higher temperatures for any partial pressure of water. In line with this observation, we find that hydration is more favorable at lower temperatures and higher partial pressures of H_2O. Calculations predict that hydration of $Na_2Fe_2(SO_4)_3$ is possible at room temperature (T = 20 °C). Overall, our calculations indicate that reaction in eq 12 might be possible at standard conditions and even at higher temperatures, although its respective free energies might be quite small (Figure 6, the boundary between the red and blue regions crosses the black solid line in the vicinity of T = 30 °C).

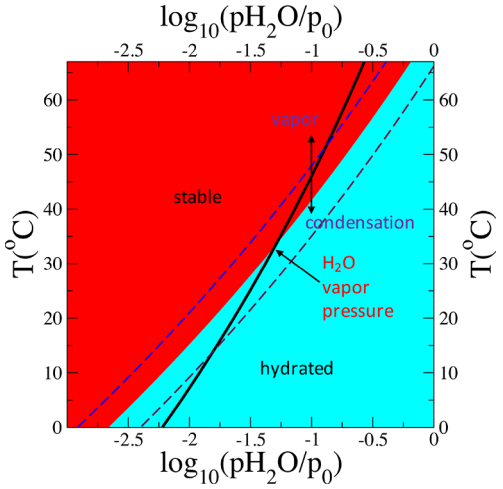

Figure 6. Diagram of $Na_2Fe_2(SO_4)_3$ stability with respect to hydration. The stable (red) and hydrated (blue) regions correspond to the temperatures and partial pressures of H_2O where the combined free energy of respective species (eq 12) is lower. The presense of the gas phase water molecules is only possible for p and T to the left of the solid black line (H_2O vapor pressure). The broken lines show the variation of the boundary between the stable and hydrated regions upon changing the total energy of $Na_2Fe_2(SO_4)_3$ (sensitivity test, see the text for details).

To analyze the sensitivity of our findings with respect to the input energies of the studied materials, we varied the total energy of $Na_{18}Fe_{15}(SO_4)_{24}$ unit in eq 12 by ±0.5 eV (this corresponds to the changes of the redox potential by about ±0.03 V). The broken lines in Figure 6 show the possible boundaries between stable and hydrated regimes (red and blue areas) upon such slight changes of the redox potential. One can see concomitant shifts of the boundary line by about ±5 °C (Figure 6), which gives an estimate of the dependence of predicted temperature of hydration from the total energies of the sulfate species in eq 12.

In addition to the analysis of a high potential $Na_2Fe_2(SO_4)_3$ cathode, we also analyzed stability of the $Na_2Fe(SO_4)_2{\cdot}2(H_2O)$ cathode material (optimized structure is shown in Figure 7), which can also be hydrated via the following reaction:

$$Na_2Fe(SO_4)_2{\cdot}2(H_2O) + 2g\,H_2O \rightarrow Na_2Fe(SO_4)_2{\cdot}4(H_2O) \quad (13)$$

Figure 8 presents a diagram analogous to that provided for hydration of $Na_2Fe_2(SO_4)_3$ (Figure 6). We find that hydration

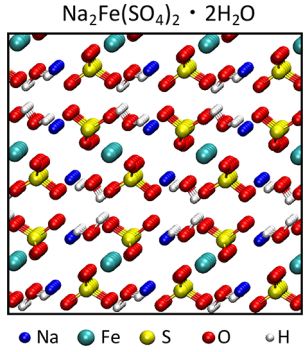

Figure 7. Optimized structure of $Na_2Fe(SO_4)_2{\cdot}2(H_2O)$.

DOI: 10.1021/acs.jpcc.7b02479
J. Phys. Chem. C 2017, 121, 20067−20074

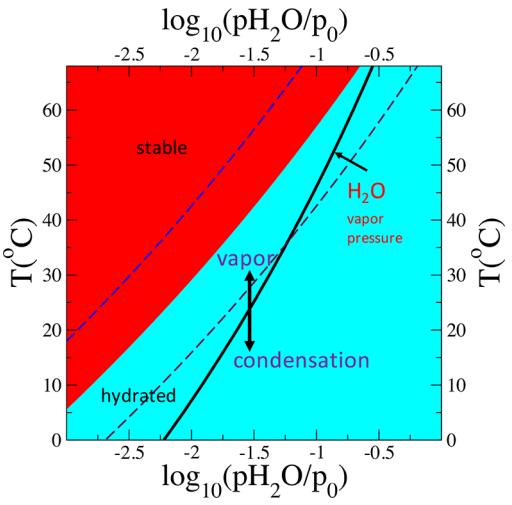

Figure 8. Diagram of $Na_2Fe(SO_4)_2{\cdot}2(H_2O)$ stability with respect to hydration. The stable and hydrated regions correspond to the temperatures and partial pressures of H_2O where the combined free energy of respective species (eq 13) is lower. The presense of the gas phase water molecules is only possible for p and T to the left of the solid black line (H_2O vapor pressure). The broken lines show the changes of the stable/hydrated boundary upon variations of $Na_2Fe(SO_4)_2{\cdot}2(H_2O)$ total energy (sensitivity test, see the text for details).

of $Na_2Fe(SO_4)_2{\cdot}2(H_2O)$ is also thermodynamically favorable at somewhat higher temperatures and lower partial pressures of water as compared to $Na_2Fe_2(SO_4)_3$. We have also performed an analysis of sensitivity of the free energy of the reaction in eq 13 with respect to the calculated total energy of $Na_2Fe(SO_4)_2{\cdot}2(H_2O)$ unit. The broken lines show variations of the stable/hydrated boundary upon changes of the redox potential of $Na_2Fe(SO_4)_2{\cdot}2(H_2O)$ by ±0.06 eV (the total energy of the supercell of $Na_2Fe(SO_4)_2{\cdot}2(H_2O)$ varies by ±0.5 eV in this case). We find that such changes in calculated redox potential result in concomitant variations of the predicted temperatures of $Na_2Fe(SO_4)_2{\cdot}2(H_2O)$ hydration by about ±10 °C. This observation shows a similar degree of sensitivity of the accuracy of predicted conditions of hydration (T and pH_2O) for the two studied cathode materials.

4. CONCLUSIONS

An ability of computational methods to adequately predict the conditions of decomposition and hydration of iron sulfate materials has been tested in this work. For this purpose, we performed calculations of the ground state properties of studied materials (i.e., enthalpies of oxidation, redox potentials, and magnetic moments of Fe cations) for comparison with available experimental data. We found that the closest agreement with experiment can be obtained when DFT+U/magnetic exchange method is employed. Particularly, the enthalpy of Fe_3O_4 oxidation with formation of Fe_2O_3 (these oxides are the products of $Na_2Fe_2(SO_4)_3$ decomposition) alongside with the magnetic moments of Fe cations have been calculated in very good agreement with experiment. Moreover, the redox potential of the product of hydration of studied sulfate materials ($Na_2Fe(SO_4)_2{\cdot}4(H_2O)$) has been also calculated with a reasonable accuracy when DFT+U/magnetic exchange method is employed. Additionally, we should note that our previous work[22] demonstrated that application of DFT+U/magnetic exchange method allows quite accurate calculation of the redox potentials of sulfate materials, whose stability we analyzed herein (i.e., $Na_2Fe_2(SO_4)_3$ and $Na_2Fe(SO_4)_2{\cdot}2(H_2O)$).

Using these benchmarked energies of the studied materials, we determined the conditions of $Na_2Fe_2(SO_4)_3$ decomposition into Na_2SO_4, Fe_2O_3, Fe_3O_4, SO_2, and O_2. Our calculations predict a low thermal stability of $Na_2Fe_2(SO_4)_3$ with the temperature $T \sim 320$ °C required for decomposition. This temperature is below experimentally reported value ($T = 450$ °C),[5] which might be explained by two possible reasons: (a) kinetic barriers associated with decomposition reaction steps might be quite high, thus requiring higher temperature for $Na_2Fe_2(SO_4)_3$ decomposition; (b) the total energies of Na_2SO_4 and SO_2 species calculated by PBE method might require additional corrections, which in turn may change the temperature of decomposition.

The temperature and partial pressure of H_2O in the air required for hydration of $Na_2Fe_2(SO_4)_3$ and $Na_2Fe(SO_4)_2{\cdot}2(H_2O)$ cathode materials have been also studied. We found that $Na_2Fe_2(SO_4)_3$ is thermodynamically unstable at room temperature ($T = 20$ °C) and even at $T > 20$ °C at high relative humidity (close to 100%). This result is in a general agreement with experiment, where $Na_2Fe_2(SO_4)_3$ is found to undergo hydration upon exposure to air.[5] Moreover, we have found that $Na_2Fe(SO_4)_2{\cdot}2(H_2O)$ cathode material can also be hydrated due to interactions with water molecules present in the air.

In summary, our work shows that analysis of stability of sulfate materials, performed with the help of DFT+U/magnetic exchange method, can provide useful and reasonably reliable information about conditions of thermal decomposition and hydration of these materials. The possible factors responsible for limitations of the applied technique and inaccuracies in prediction of the studied properties of interest (e.g., underestimated temperature of $Na_2Fe_2(SO_4)_3$ decomposition) have been highlighted and discussed.

AUTHOR INFORMATION

Corresponding Author

shishkin.maxim.6c@kyoto-u.ac.jp

ORCID

Maxim Shishkin: 0000-0001-6010-7916

Hirofumi Sato: 0000-0001-6266-9058

Notes

The authors declare no competing financial interest.

ACKNOWLEDGMENTS

This work was performed under a management of Elements Strategy Initiative for Catalysts and Batteries (ESICB); financial support is acknowledged.

REFERENCES

(1) Reynaud, M.; Ati, M.; Melot, B. C.; Sougrati, M. T.; Rousse, G.; Chotard, J.-N.; Tarascon, J.-M. $Li_2Fe(SO_4)_2$ as a 3.83 V positive electrode material. *Electrochem. Commun.* **2012**, *21*, 77−80.

(2) Barpanda, P.; Ati, M.; Melot, B. C.; Rousse, G.; Chotard, J.-N.; Doublet, M.-L.; Sougrati, M. T.; Corr, S.; Jumas, J.-C.; Tarascon, J.-M. A 3.90 V iron-based fluorosulphate material for lithium-ion batteries crystallizing in the triplite structure. *Nat. Mater.* **2011**, *10*, 772−779.

(3) Ati, M.; Melot, B.; Chotard, J.-N.; Rousse, G.; Reynaud, M.; Tarascon, J.-M. Synthesis and electrochemical properties of pure $LiFeSO_4F$ in the triplite structure. *Electrochem. Commun.* **2011**, *13*, 1280−1283.

DOI: 10.1021/acs.jpcc.7b02479
J. Phys. Chem. C 2017, 121, 20067−20074

(4) Barpanda, P. Sulfate Chemistry for High-Voltage Insertion Materials: Synthetic, Structural and Electrochemical Insights. *Isr. J. Chem.* **2015**, *55*, 537−557.
(5) Barpanda, P.; Oyama, G.; Nishimura, S.; Chung, S.-C.; Yamada, A. A 3.8-V earth-abundant sodium battery electrode. *Nat. Commun.* **2014**, *5*, 4358.1−4358.8.
(6) Marinova, D.; Kostov, V.; Nikolova, R.; Kukeva, R.; Zhecheva, E.; Sendova-Vasileva, M.; Stoyanova, R. From kröhnkite- to alluaudite-type of structure: novel method of synthesis of sodium manganese sulfates with electrochemical properties in alkali- metal ion batteries. *J. Mater. Chem. A* **2015**, *3*, 22287−22299.
(7) Dwibedi, D.; Gond, R.; Dayamani, A.; Araujo, R. B.; Chakraborty, S.; Ahuja, R.; Barpanda, P. $Na_{2.32}Co_{1.84}(SO_4)_3$ as a new member of the alluaudite family of high-voltage sodium battery cathodes. *Dalton Transations* **2017**, *46*, 55−63.
(8) Kulik, H. J. Perspective: Treating electron over-delocalization with the DFT+*U* method. *J. Chem. Phys.* **2015**, *142*, 240901.1−240901.10.
(9) Anisimov, V.; Izyumov, Y. *Electronic Structure of Strongly Correlated Materials*, 1st ed.; Springer Series in Solid-State Sciences: New York, 2010.
(10) Wang, L.; Maxisch, T.; Ceder, G. Oxidation energies of transition metal oxides within the GGA+*U* framework. *Phys. Rev. B: Condens. Matter Mater. Phys.* **2006**, *73*, 195107.1−195107.6.
(11) Jain, A.; Hautier, G.; Ong, S. P.; Moore, C. J.; Fischer, C. C.; Persson, K. A.; Ceder, G. Formation enthalpies by mixing GGA and GGA+*U* calculations. *Phys. Rev. B: Condens. Matter Mater. Phys.* **2011**, *84*, 045115.1−045115.10.
(12) Aykol, M.; Wolverton, C. Local environment dependent GGA +*U* method for accurate thermochemistry of transition metal compounds. *Phys. Rev. B: Condens. Matter Mater. Phys.* **2014**, *90*, 115105.1−115105.18.
(13) Deml, A. M.; O'Hayre, R.; Wolverton, C.; Stevanovic, V. Predicting density functional theory total energies and enthalpies of formation of metal-nonmetal compounds by linear regression. *Phys. Rev. B: Condens. Matter Mater. Phys.* **2016**, *93*, 085142.1−085142.9.
(14) Zhou, F.; Cococcioni, M.; Marianetti, C. A.; Morgan, D.; Ceder, G. First-principles prediction of redox potentials in transition-metal compounds with LDA+*U*. *Phys. Rev. B: Condens. Matter Mater. Phys.* **2004**, *70*, 235121.1−235121.8.
(15) Mosey, N. J.; Carter, E. A. Ab initio evaluation of Coulomb and exchange parameters for DFT+*U* calculations. *Phys. Rev. B: Condens. Matter Mater. Phys.* **2007**, *76*, 155123.1−155123.13.
(16) Mosey, N. J.; Liao, P.; Carter, E. M. Rotationally invariant ab initio evaluation of Coulomb and exchange parameters for DFT+*U* calculations. *J. Chem. Phys.* **2008**, *129*, 014103.1−014103.13.
(17) Agapito, L. A.; Curtarolo, S.; BuongiornoNardelli, M. Reformulation of DFT+*U* as a Pseudohybrid Hubbard Density Functional for Accelerated Materials Discovery. *Phys. Rev. X* **2015**, *5*, 011006.1−011006.16.
(18) Aryasetiawan, F.; Karlsson, K.; Jepsen, O.; Schönberger, U. Calculations of Hubbard U from first-principles. *Phys. Rev. B: Condens. Matter Mater. Phys.* **2006**, *74*, 125106.1−125106.9.
(19) Karlsson, K.; Aryasetiawan, F.; Jepsen, O. Method for calculating the electronic structure of correlated materials from a truly first-principles LDA+*U* scheme. *Phys. Rev. B: Condens. Matter Mater. Phys.* **2010**, *81*, 245113.1−245113.5.
(20) Sakuma, R.; Aryasetiawan, F. First-principles calculations of dynamical screened interactions for the transition metal oxides MO (M = Mn, Fe, Co, Ni). *Phys. Rev. B: Condens. Matter Mater. Phys.* **2013**, *87*, 165118.1−165118.8.
(21) Shishkin, M.; Sato, H. Self-consistent parametrization of DFT + *U* framework using linear response approach: Application to evaluation of redox potentials of battery cathodes. *Phys. Rev. B: Condens. Matter Mater. Phys.* **2016**, *93*, 085135.1−085135.13.
(22) Shishkin, M.; Sato, H. Challenges in computational evaluation of redox and magnetic properties of Fe-based sulfate cathode materials of Li- and Na-ion batteries. *J. Phys.: Condens. Matter* **2017**, *29*, 215701.1−215701.12.
(23) http://cms.mpi.univie.ac.at/vasp/vasp/vasp.html, online; accessed 24 August 2017.
(24) Perdew, J.; Burke, K.; Ernzerhof, M. Generalized Gradient Approximation Made Simple. *Phys. Rev. Lett.* **1996**, *77*, 3865−3868.
(25) Blöchl, P. E. Projector augmented-wave method. *Phys. Rev. B: Condens. Matter Mater. Phys.* **1994**, *50*, 17953−17979.
(26) Kresse, G.; Joubert, D. From ultrasoft pseudopotentials to the projector augmented-wave method. *Phys. Rev. B: Condens. Matter Mater. Phys.* **1999**, *59*, 1758−1775.
(27) Monkhorst, H. J.; Pack, J. D. Special points for Brillouin-zone integrations. *Phys. Rev. B* **1976**, *13*, 5188−5192.
(28) Liechtenstein, A. I.; Anisimov, V. I.; Zaanen, J. Density-functional theory and strong interactions: Orbital ordering in Mott-Hubbard insulators. *Phys. Rev. B: Condens. Matter Mater. Phys.* **1995**, *52*, R5467−R5470.
(29) Dudarev, S. L.; Botton, G. A.; Savrasov, S. Y.; Humphreys, C. J.; Sutton, A. P. Electron-energy-loss spectra and the structural stability of nickel oxide: An LSDA+*U* study. *Phys. Rev. B: Condens. Matter Mater. Phys.* **1998**, *57*, 1505−1509.
(30) Cococcioni, M.; de Gironcoli, S. Linear response approach to the calculation of the effective interaction parameters in the LDA+*U* method. *Phys. Rev. B: Condens. Matter Mater. Phys.* **2005**, *71*, 035105.1−035105.16.
(31) Himmetoglu, B.; Wentzcovitch, R. W.; Cococcioni, M. First-principles study of electronic and structural properties of CuO. *Phys. Rev. B: Condens. Matter Mater. Phys.* **2011**, *84*, 115108.1−115108.8.
(32) Shishkin, M.; Sato, H. Erratum: "Challenges in computational evaluation of redox and magnetic properties of Fe-based sulfate cathode materials of Li- and Na-ion batteries" J. of Phys.: Condens. Matter 29, 215701 (2017). *J. Phys.: Condens. Matter* **2017**, *29*, 215701.
(33) Guo, Y.; Clark, S. J.; Robertson, J. Electronic and magnetic properties of Ti_2O_3, Cr_2O_3, and Fe_2O_3 calculated by the screened exchange hybrid density functional. *J. Phys.: Condens. Matter* **2012**, *24*, 325504.1−325504.8.
(34) Wenzel, M. J.; Steinle-Neumann, G. Nonequivalence of the octahedral sites of cubic Fe_3O_4 magnetite. *Phys. Rev. B: Condens. Matter Mater. Phys.* **2007**, *75*, 21443.01−21443.06.
(35) http://www.wiredchemist.com/chemistry/data/entropies-inorganic, online; accessed 24 August 2017.
(36) Johnston, K.; Castell, M. R.; Paxton, A. T.; Finnis, M. W. $SrTiO_3$(001)2 × 1 reconstructions: First-principles calculations of surface energy and atomic structure compared with scanning tunneling microscopy images. *Phys. Rev. B: Condens. Matter Mater. Phys.* **2004**, *70*, 085415.1−085415.12.
(37) Shishkin, M.; Ziegler, T. Structural, electronic, stability and reduction properties of perovskite surfaces: The case of rhombohedral $BaCeO_3$. *Surf. Sci.* **2012**, *606*, 1078−1087.
(38) https://www.webelements.com/oxygen/thermochemistry.html, online; accessed 24 August 2017.
(39) Lee, Y.; Kleis, J.; Rossmeisl, J.; Morgan, D. Ab initio energetics of $LaBO_3$(001) (B = Mn, Fe, Co, and Ni) for solid oxide fuel cell cathodes. *Phys. Rev. B: Condens. Matter Mater. Phys.* **2009**, *80*, 224101.1−224101.20.
(40) Huang, D.; Chang, C.; Jeng; Guo, G.; Lin, H.-J.; Wu, W. B.; Ku, H.; Fujimori, A.; Takahashi, Y.; Chen, C. Spin and Orbital Magnetic Moments of Fe_3O_4. *Phys. Rev. Lett.* **2004**, *93*, 077204.1−077204.4.
(41) Heifets, E.; Ho, J.; Merinov, B. Density functional simulation of the $BaZrO_3$ (011) surface structure. *Phys. Rev. B: Condens. Matter Mater. Phys.* **2007**, *75*, 155431.1−155431.15.
(42) Reuter, K.; Scheffler, M. Composition, structure, and stability of RuO_2(110) as a function of oxygen pressure. *Phys. Rev. B: Condens. Matter Mater. Phys.* **2001**, *65*, 035406.1−035406.11.
(43) Fournier, R.; Boroukhovskaia, L. Accurate energies calculated by empirical corrections to the local spin density approximation. *Theor. Chem. Acc.* **2004**, *112*, 1−6.
(44) Reynaud, M. *Design of new sulfate-based positive electrode materials for Li- and Na-ion batteries*, Ph.D. thesis, Université de Picardie Jules Verne, 2014.

DOI: 10.1021/acs.jpcc.7b02479
J. Phys. Chem. C 2017, 121, 20067−20074